INSTITUTE OF PHYSICS PUBLISHING SMART MATERIALS AND STRUCTURES
Smart Mater. Struct. **13** (2004) 1118–1130 PII: S0964-1726(04)83417-7

A nonlinear finite element method applied to shape memory bars

Carlos Américo P L La Cava[1], **Marcelo A Savi**[2] **and Pedro Manuel C L Pacheco**[3]

[1] Volkswagen South America—Truck and Bus, Engenharia Avançada e Protótipos, 27.501.970-Resende, RJ, Brazil
[2] COPPE—Department of Mechanical Engineering, Universidade Federal do Rio de Janeiro, Caixa Postal 68.503, 21.945.970-Rio de Janeiro, RJ, Brazil
[3] Department of Mechanical Engineering, CEFET/RJ, 20.271.110-Rio de Janeiro, RJ, Brazil

E-mail: Carlos.LaCava@volkswagen.com.br, savi@ufrj.br and calas@cefet-rj.br

Received 23 October 2003, in final form 17 June 2004
Published 11 August 2004
Online at stacks.iop.org/SMS/13/1118
doi:10.1088/0964-1726/13/5/017

Abstract
This contribution is concerned with the analysis of the nonlinear behavior of shape memory bars, employing the finite element method. A constitutive equation based on Fremond's theory is considered. The proposed constitutive model considers four phases in the formulation (three variants of martensite and an austenitic phase), including thermal expansion and plastic strains. An iterative numerical process based on an operator split technique is developed in order to deal with the nonlinearities of the formulation. On this basis, coupled governing equations can be solved from uncoupled problems where classical procedures can be employed. Numerical simulations are carried out in order to illustrate the general behavior of shape memory bars under different thermomechanical loadings. Results show that the proposed model captures the general behavior of SMAs, allowing the description of bars subjected to non-homogeneous thermomechanical loads.

(Some figures in this article are in colour only in the electronic version)

1. Introduction

Shape memory alloys (SMAs) are found in a great number of applications in different fields of science and engineering. Self-actuating fasteners (La Cava *et al* 2000, van Humbeeck 1999, Kibirkstis *et al* 1997, Borden 1991), thermal actuator switches and several bioengineering devices provide some examples of such applications (Machado and Savi 2002, 2003, Duerig *et al* 1999, Lagoudas *et al* 1999). Aerospace technology is also using SMAs for solve important problems, in particular those concerning space saving achieved with self-erectable structures, stabilizing mechanisms and non-explosive release devices (Pacheco and Savi 1997, Denoyer *et al* 2000). Micromanipulators and robotic actuators have been built employing SMA properties to mimic the smooth motions of human muscles (Garner *et al* 2001, Webb *et al* 2000, Fujita and Toshiyoshi 1998, Rogers 1995). Moreover, SMAs are being used as actuators for vibration and buckling control for flexible structures (Pietrzakowski 2000, Birman 1997, Rogers 1995). Despite all these applications, the modeling of SMAs is still the object of much research carried out in order to obtain a full description of the details of their thermomechanical behavior.

This contribution proposes a finite element (FE) formulation for dealing with shape memory bars. Finite element modeling of SMA structures has previously been addressed by Brinson and Lammering (1993): a constitutive theory based on Tanaka's model (Tanaka 1986), and later modified by Brinson (1993), was employed to describe the SMA behavior. More recently, Auricchio and Taylor (1996) have also proposed a three-dimensional finite element model. Savi *et al* (1998) discuss an iterative numerical procedure that has been developed to deal with both geometrical and constitutive nonlinearities in the finite element model for adaptive trusses with SMA actuators. Lagoudas *et al* (1997) consider the thermomechanical response of a laminate with

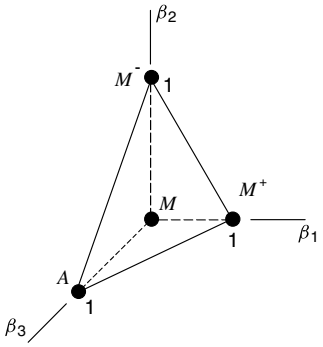

Figure 1. The tetrahedron of the constraints, π.

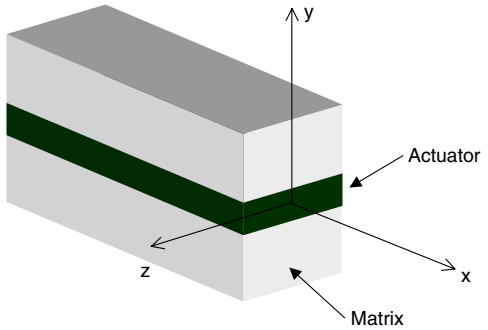

Figure 2. A composite bar with a SMA actuator.

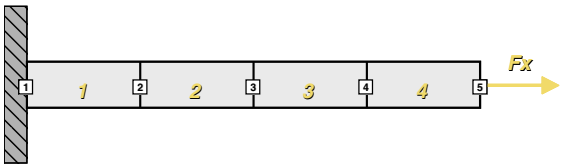

Figure 3. A SMA bar subjected to a homogeneous axial load process.

SMA strips where the thermomechanical response is based on the Boyd–Lagoudas polynomial hardening model (Boyd and Lagoudas 1996). Kouzak *et al* (1998) also treats SMA beams using a constitutive equation proposed by Brinson (1993). Trochu and Qian (1997), Masud *et al* (1997), Bhattacharyya *et al* (2000), Liu *et al* (2002) are other contributions in this field. Moreover, dual kriging interpolation has been employed with a finite element method (FEM) in order to describe the shape memory behavior (Trochu and Qian 1997, Trochu and Terriault 1998, Trochu *et al* 1999).

Here, the finite element method is employed, facilitating the spatial discretization of bars using a constitutive model proposed by Savi *et al* (2002) and Baêta-Neves *et al* (2004) to describe the thermomechanical behavior of SMAs. The main goal is the use of the classical FEM associated with a constitutive model that represents the general thermomechanical behavior of SMAs. The tool developed allows one to describe the general behavior of SMA bars subjected to non-homogeneous thermomechanical loads using well-established numerical procedures.

The constitutive model is based on Fremond's theory (Fremond 1987, 1996) and includes four phases in the formulation: three variants of martensite and an austenitic phase. Furthermore, different material parameters for the austenitic and martensitic phases are involved. Thermal expansion and plastic strains are also included in the formulation and the hardening effect is represented by a combination of kinematic and isotropic behaviors. A plastic phase transformation coupling is incorporated into the model allowing a correct description of the thermomechanical behavior of SMAs. Moreover, horizontal enlargement of the stress–strain hysteresis loop is considered, allowing better adjustments with experimental data.

An iterative numerical procedure based on an operator split technique (Ortiz *et al* 1983) is developed in order to deal with the nonlinearities in the formulation. On this basis, coupled governing equations can be solved from uncoupled problems where classical numerical procedures can be employed. Numerical simulations are carried out, revealing the different behaviors of SMA bars. The results show that the proposed model is able to capture the general behavior of SMAs, including pseudoelastic behavior, shape memory effects and phase transformations due to temperature variations.

2. Constitutive model

The description of the thermomechanical behavior of SMAs has been the objective of much recent research. In this paper, the constitutive model proposed by Savi *et al* (2002) and Baêta-Neves *et al* (2004), which is built upon the Fremond model (Fremond 1987, 1996), is employed in order to describe the SMA behavior.

The proposed model is constructed within the scope of the standard generalized material approach (Lemaitre and Chaboche 1990) considering one-dimensional media. On this basis, the thermomechanical behavior can be described in terms of the Helmholtz free energy, ψ, and the dual of the pseudopotential of dissipation, ϕ^*, automatically satisfying the second law of thermodynamics. Here, a brief description of the constitutive model is presented. A more detailed description of this model may be found in Savi *et al* (2002) and Baêta-Neves *et al* (2004).

The description of the thermomechanical behavior of SMAs is given, considering the following state variables: strain, ε; temperature, T; the volumetric fractions of the martensitic variants β_1 and β_2, which are associated with detwinned martensites (M^+ and M^-, respectively), and the austenite (A), β_3. The fourth phase is associated with twinned martensite (M) and its volumetric fraction is β_4. Notice, however, that the variable β_4 can be eliminated since $\beta_1 + \beta_2 + \beta_3 + \beta_4 = 1$. The plasticity phenomenon is described considering classical plasticity with the aid of the plastic strain, ε^{p}, and the hardening effect is represented by a combination of kinematic and isotropic behaviors, described using variables μ and γ, respectively. Additive decomposition is assumed and the constitutive model may be presented as follows:

$$\sigma = E(\varepsilon - \varepsilon^{\mathrm{p}}) + (\alpha + E\alpha_{\mathrm{H}})(\beta_2 - \beta_1) - \Omega(T - T_0) \tag{1}$$

$$\dot{\beta}_1 = \frac{1}{\eta}\Bigg[\alpha(\varepsilon - \varepsilon^{\mathrm{p}}) + \frac{L_{\mathrm{M}}}{T_{\mathrm{M}}}(T - T_{\mathrm{M}}) + \alpha_{\mathrm{H}}\left[E(\varepsilon - \varepsilon^{\mathrm{p}}) + (2\alpha + E\alpha_{\mathrm{H}})(\beta_2 - \beta_1) - \Omega(T - T_0)\right] - \eta_{\mathrm{ci}} K\gamma - \eta_{\mathrm{ck}}\frac{\mu}{H} - \partial_1 J\Bigg] \tag{2}$$

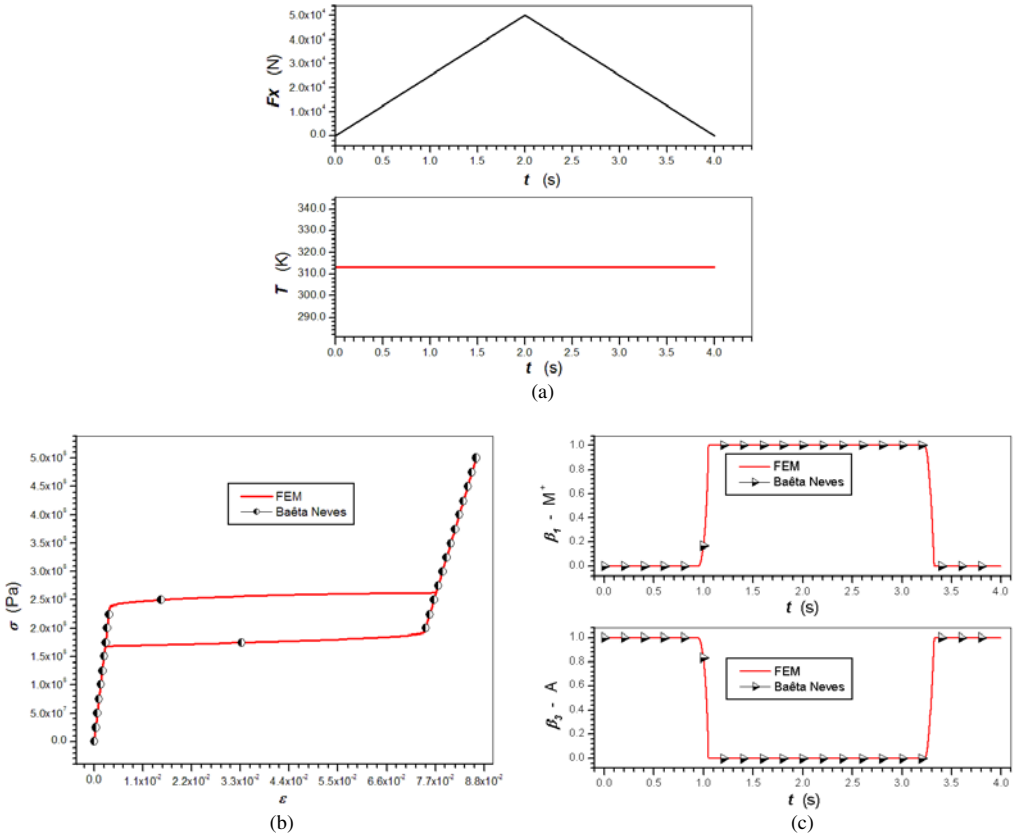

Figure 4. Pseudoelasticity. (a) Thermomechanical loading. (b) The stress–strain curve. (c) Volumetric fractions of phases.

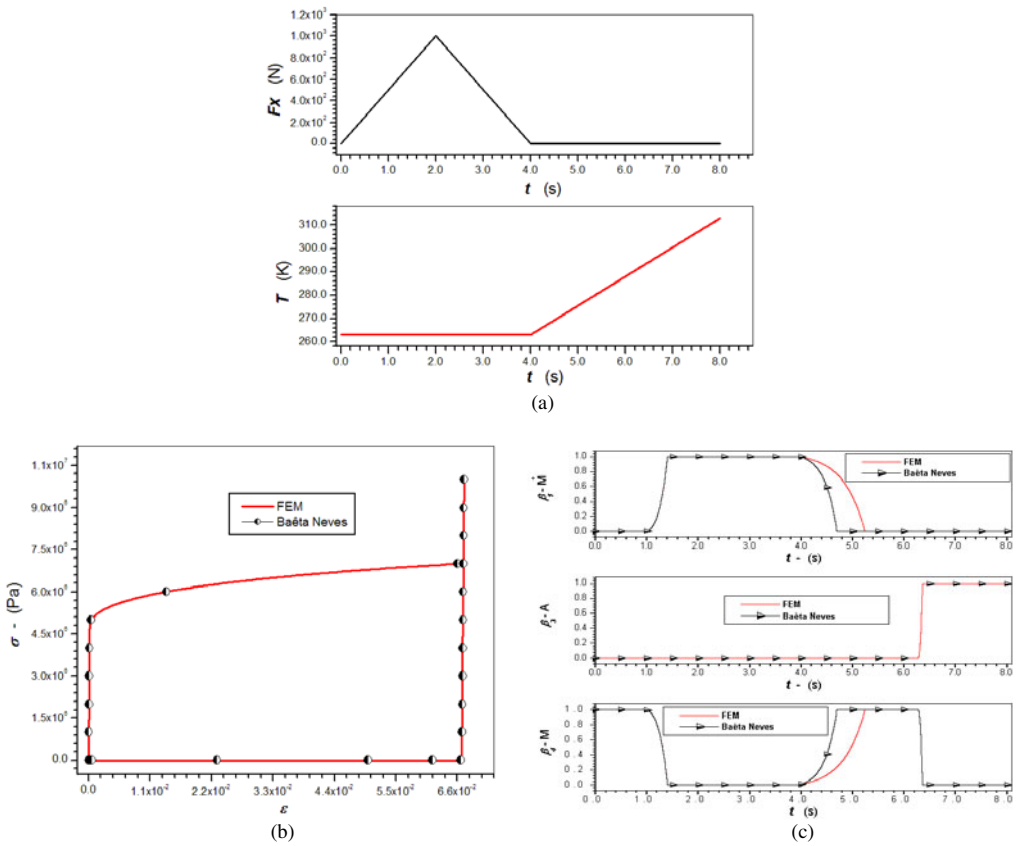

Figure 5. The shape memory effect. (a) Thermomechanical loading. (b) The stress–strain curve. (c) Volumetric fractions of phases.

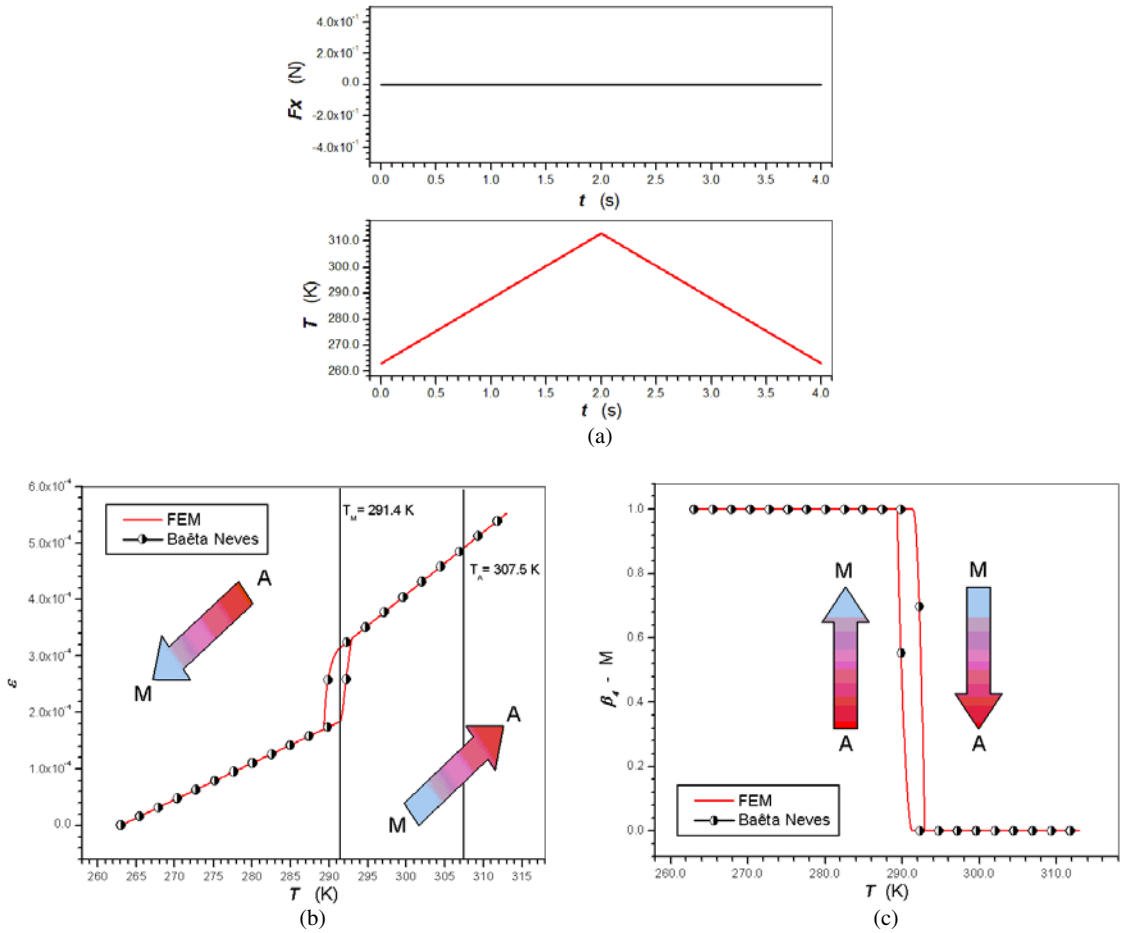

Figure 6. The phase transformation due to temperature variation. (a) Thermomechanical loading. (b) The strain–temperature curve. (c) Volumetric fractions of phases.

$$\dot{\beta}_2 = \frac{1}{\eta}\Big[-\alpha(\varepsilon - \varepsilon^{\mathrm{p}}) + \frac{L_{\mathrm{M}}}{T_{\mathrm{M}}}(T - T_{\mathrm{M}}) - \alpha_{\mathrm{H}}\left[E(\varepsilon - \varepsilon^{\mathrm{p}}) + (2\alpha + E\alpha_{\mathrm{H}})(\beta_2 - \beta_1) - \Omega(T - T_0)\right] - \eta_{\mathrm{ci}} K\gamma - \eta_{\mathrm{ck}}\frac{\mu}{H} - \partial_2 J\Big] \tag{3}$$

$$\dot{\beta}_3 = \frac{1}{\eta}\Big[-\frac{1}{2}(E_{\mathrm{A}} - E_{\mathrm{M}})[(\varepsilon - \varepsilon^{\mathrm{p}}) - \alpha_{\mathrm{H}}(\beta_1 - \beta_2)]^2 + \frac{(L_{\mathrm{M}} + L_{\mathrm{A}})}{T_{\mathrm{M}}}(T - T_{\mathrm{M}}) + (\Omega_{\mathrm{A}} - \Omega_{\mathrm{M}})(T - T_0) \times [(\varepsilon - \varepsilon^{\mathrm{p}}) - \alpha_{\mathrm{H}}(\beta_1 - \beta_2)] - \tfrac{1}{2}(K_{\mathrm{A}} - K_{\mathrm{M}})\gamma^2 - \left(\frac{1}{2H_{\mathrm{A}}} - \frac{1}{2H_{\mathrm{M}}}\right)\mu^2 + \eta_{\mathrm{ci}} K\gamma + \eta_{\mathrm{ck}}\frac{\mu}{H} - \partial_3 J\Big] \tag{4}$$

$$\dot{\varepsilon}^{\mathrm{p}} = \lambda\,\mathrm{sgn}(\sigma - \mu) \tag{5}$$

$$\dot{\gamma} = |\dot{\varepsilon}^{\mathrm{p}}| + \eta_{\mathrm{ci}}(\dot{\beta}_1 + \dot{\beta}_2 - \dot{\beta}_3) \tag{6}$$

$$\dot{\mu} = H\dot{\varepsilon}^{\mathrm{p}} + \eta_{\mathrm{ck}}(\dot{\beta}_1 + \dot{\beta}_2 - \dot{\beta}_3) \tag{7}$$

where: σ is the stress; α, $L_{\mathrm{M}} = L_{\mathrm{M}}(T)$ and $L_{\mathrm{A}} = L_{\mathrm{A}}(T)$ are material parameters that are used to describe the martensitic transformation; E_{M} and E_{A} represent the elastic moduli for the martensitic and austenitic phases, respectively; Ω_{M} and Ω_{A} represent the thermal expansion coefficients for martensitic and austenitic phases, respectively; K_{M} and K_{A} are the plastic moduli for martensitic and austenitic phases while H_{M} and H_{A} are the kinematic hardening moduli for martensitic and austenitic phases; T_{M} is a temperature below which the martensitic phase starts its formation in the absence of stress while T_0 is a reference temperature; ρ is the density. The parameter α_{H} defines the horizontal width of the stress–strain hysteresis loop. On the other hand, the parameter η is associated with the internal dissipation of the material while η_{ci} and η_{ck} are related to plastic phase transformation coupling. The parameter η_{ci} is associated with isotropic hardening coupling while η_{ck} is associated with kinematic hardening coupling. Moreover, λ is the classical plastic multiplier and the following definitions are assumed in the previous equations:

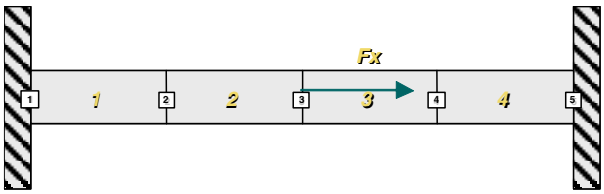

Figure 7. A bar subjected to an axial load at the mid-point and restricted at both ends.

$$E = E_{\mathrm{M}} - \beta_3(E_{\mathrm{M}} - E_{\mathrm{A}}) \tag{8}$$

$$\Omega = \Omega_{\mathrm{M}} - \beta_3(\Omega_{\mathrm{M}} - \Omega_{\mathrm{A}}) \tag{9}$$

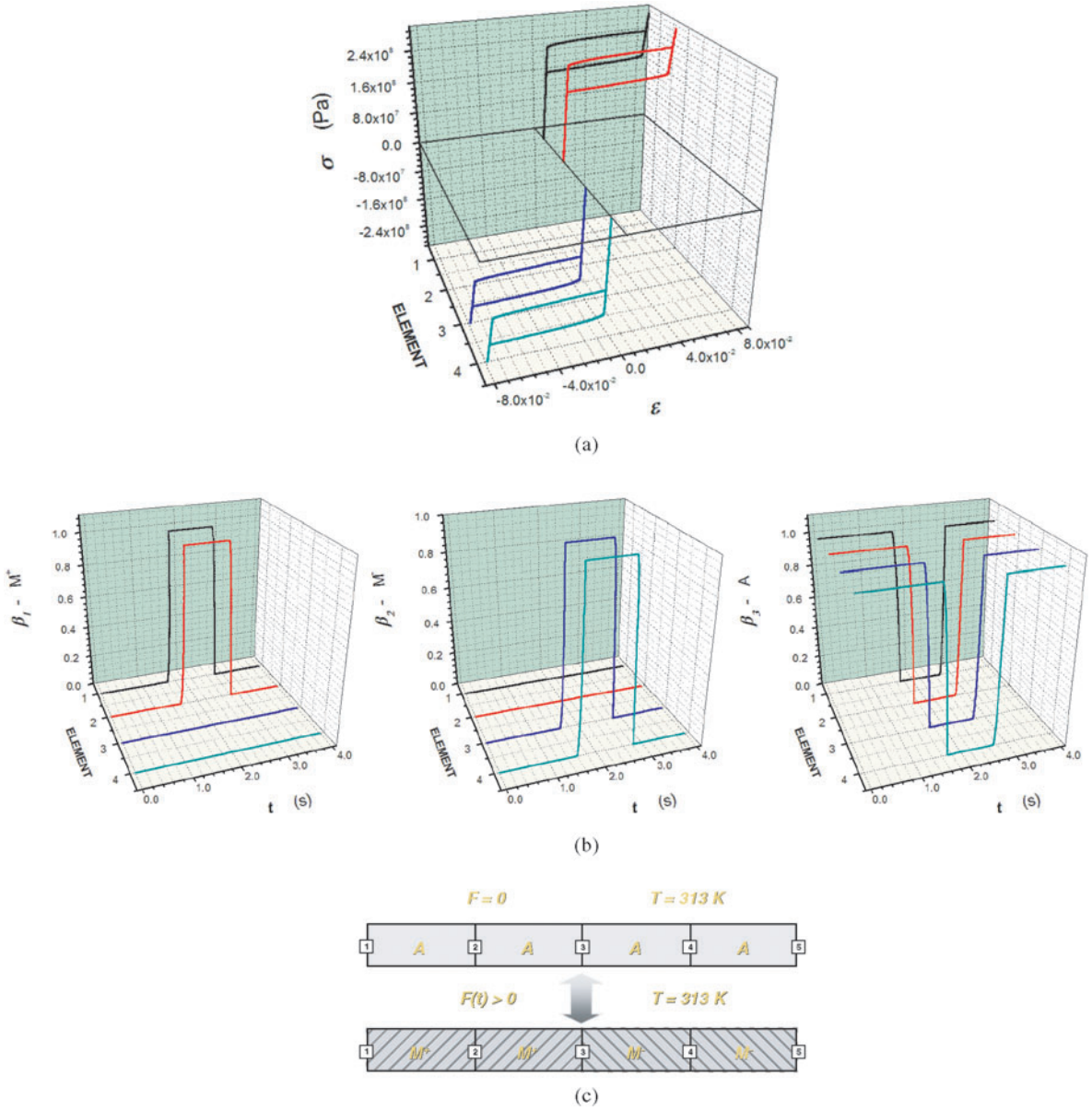

Figure 8. The pseudoelastic effect for a bar subjected to an axial load at the mid-point and restricted at both ends. (a) Stress–strain curves. (b) Volumetric fractions of phases. (c) A schematic representation of the phase distribution.

$$K = K_{\mathrm{M}} - \beta_3(K_{\mathrm{M}} - K_{\mathrm{A}}) \tag{10}$$

$$\frac{1}{H} = \frac{1}{H_{\mathrm{M}}} - \beta_3\left(\frac{1}{H_{\mathrm{M}}} - \frac{1}{H_{\mathrm{A}}}\right). \tag{11}$$

The definitions of the parameters L_{M} and L_{A} are associated with a material parameter L and a temperature T_{C}, defined as the temperature below which there is no change in the stress–strain hysteresis loop position. This definition is introduced with the objective of limiting the displacement of the hysteresis loop with respect to temperature when $T < T_{\mathrm{C}}$. The following expressions are obtained:

$$L_{\mathrm{M}}(T) = \begin{cases} L_{\mathrm{M}} = L & \text{if } T \geqslant T_{\mathrm{C}} \\ L_{\mathrm{M}} = L\dfrac{(T_{\mathrm{C}} - T_{\mathrm{M}})}{(T - T_{\mathrm{M}})} & \text{if } T < T_{\mathrm{C}} \end{cases} \tag{12}$$

$$L_{\mathrm{A}}(T) = \begin{cases} L_{\mathrm{A}} = L & \text{if } T \geqslant T_{\mathrm{C}} \\ L_{\mathrm{A}} = 2L - \left[L\dfrac{(T_{\mathrm{C}} - T_{\mathrm{M}})}{(T - T_{\mathrm{M}})}\right] & \text{if } T < T_{\mathrm{C}}. \end{cases} \tag{13}$$

Moreover, $J = J(\beta_1, \beta_2, \beta_3)$ represents the indicator function of the tetrahedron π of the set (figure 1)

$$\pi = \left\{ \beta_i \in \mathrm{Re} \;\middle|\; \begin{array}{l} 0 \leqslant \beta_i \leqslant 1 (i = 1, 2, 3);\ \beta_1 + \beta_2 + \beta_3 \leqslant 1; \\ \beta_1 = \beta_2 = 0 \text{ if } \sigma = 0 \text{ and } \beta_1^{\mathrm{S}} = \beta_2^{\mathrm{S}} = 0 \end{array} \right\}. \tag{14}$$

This set also includes the constraints where detwinned martensites, M^+ and M^-, are induced by stress fields. The definition of this physical aspect is considered when $\sigma = 0$

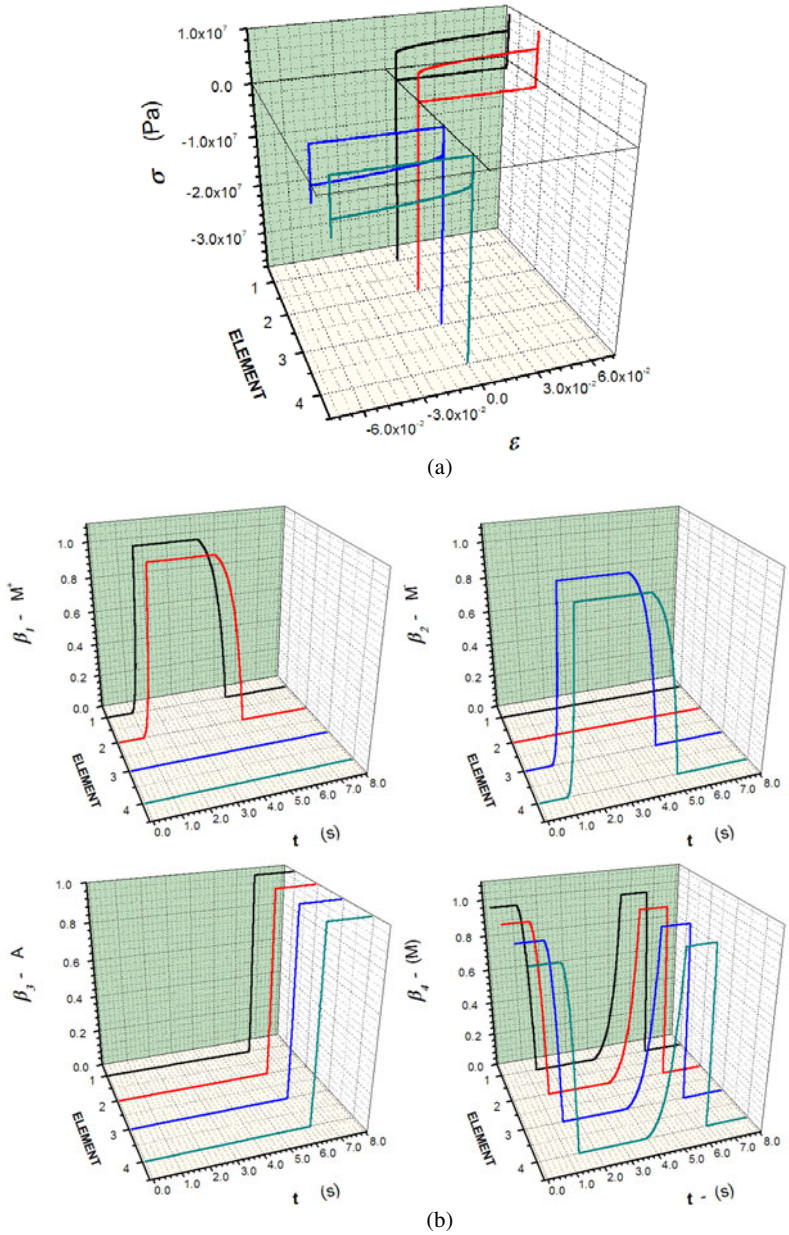

Figure 9. The shape memory effect for a bar subjected to an axial load at the mid-point and restricted at both ends. (a) Stress–strain curves. (b) Volumetric fractions of phases. (c) A schematic representation of the phase distribution.

and $\beta_1^S = \beta_2^S = 0$, where β_1^S and β_2^S are the values of β_1 and β_2, respectively, when the phase transformation begins to take place.

As regards plastic behavior, the yield surface is defined as follows (Lemaitre and Chaboche 1990):

$$f(\sigma, \mu, \gamma) = |\sigma - \mu| - (\sigma_Y + K\gamma). \tag{15}$$

The irreversible nature of plastic flow is represented by means of the *Kuhn–Tucker conditions*. Another constraint must be satisfied when $f(\sigma, \gamma, \mu) = 0$. It is referred to as the *consistency condition* and corresponds to the physical requirement that a stress point on the yield surface must persist on it. These conditions are presented as follows (Simo and Hughes 1998):

$$\begin{gathered} \lambda \geqslant 0 \qquad f(\sigma, \gamma, \mu) \leqslant 0 \qquad \lambda f(\sigma, \gamma, \mu) = 0 \\ \lambda \dot{f}(\sigma, \gamma, \mu) = 0 \qquad \text{if } f(\sigma, \gamma, \mu) = 0. \end{gathered} \tag{16}$$

The proposed model captures the general behavior of SMAs, being capable of describing pseudoelasticity, the phase transformation due to temperature variation and both one-way and two-way shape memory effects (Savi *et al* 2002).

3. Finite element formulation

In order to present the finite element formulation, we consider a composite bar reinforced with a SMA actuator (figure 2), subjected to an axial load. The actuator is assumed to have a thickness significantly less than the cross-sectional width of

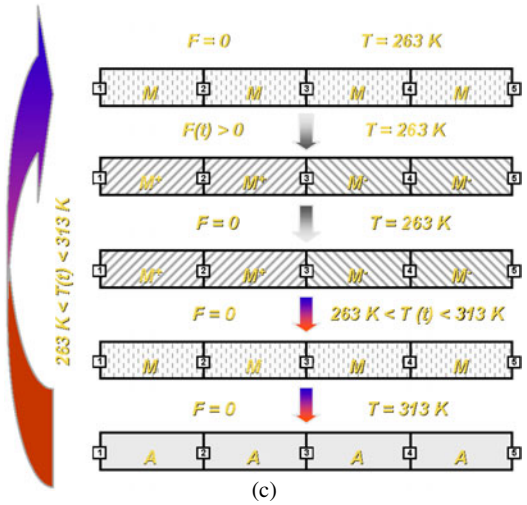

(c)

Figure 9. (Continued.)

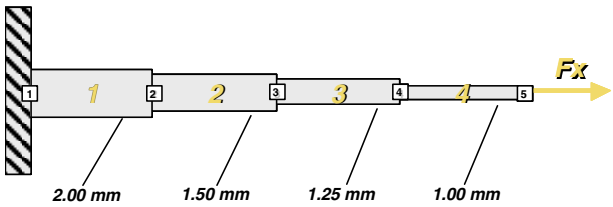

Figure 10. A bar with a variable cross-section.

the bar and also to be constructed in such a way as to preserve the symmetry of the axial load, avoiding flexure loads.

The internal energy increment may be written as follows:

$$\delta\Gamma = \int_{V_m} \sigma_m \delta\varepsilon \, dV + \int_{V_a} \sigma_a \delta\varepsilon \, dV \tag{17}$$

where V is the volume and the subscripts m and a indicate association with the matrix and the actuator, respectively. An elastic relation is considered for the matrix: $\sigma_m = E_m \varepsilon$, where E_m is the matrix elastic modulus; σ_a is given by the constitutive equation presented in the preceding section. For simplicity, a compact form of the stress–strain relation is presented here:

$$\sigma_a = E\varepsilon + \Lambda_a \tag{18}$$

where Λ_a represents the nonlinear terms related to the phase transformation and plastic behavior:

$$\Lambda_a = -E\varepsilon^p + (\alpha + E\alpha_H)(\beta_2 - \beta_1) - \Omega(T - T_0). \tag{19}$$

A kinematics equation similar to infinitesimal strain hypothesis is adopted:

$$\varepsilon = u_{,x} \tag{20}$$

where $(\,)_{,x} = \mathrm{d}(\,)/\mathrm{d}x$. Now, it is possible to consider the principle of virtual work as follows, since the term Λ_a is assumed to be constant in the actuator:

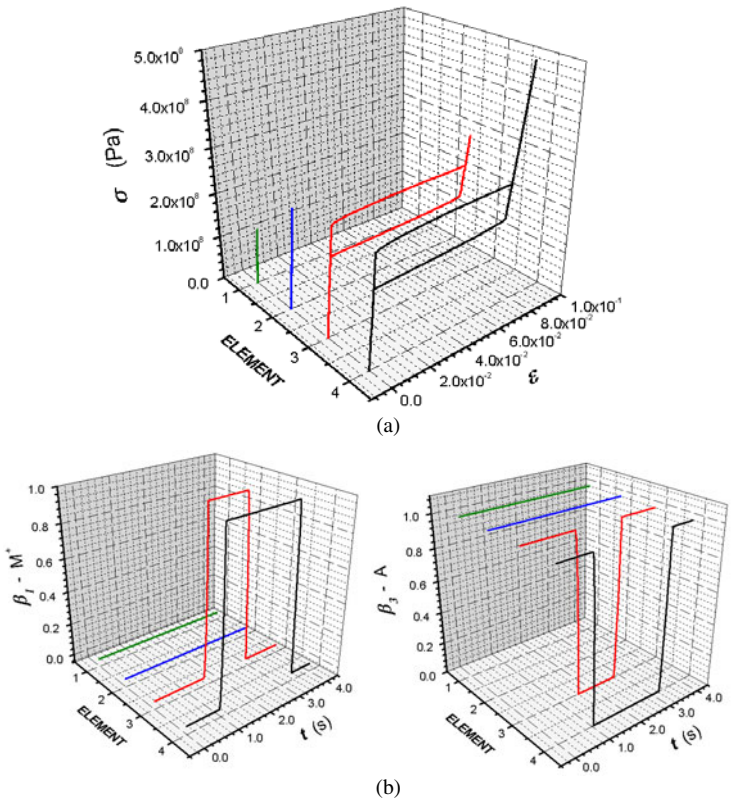

(a)

(b)

Figure 11. The pseudoelastic effect for a bar with a variable cross-section subjected to an axial load. (a) Stress–strain curves. (b) Volumetric fractions of phases.

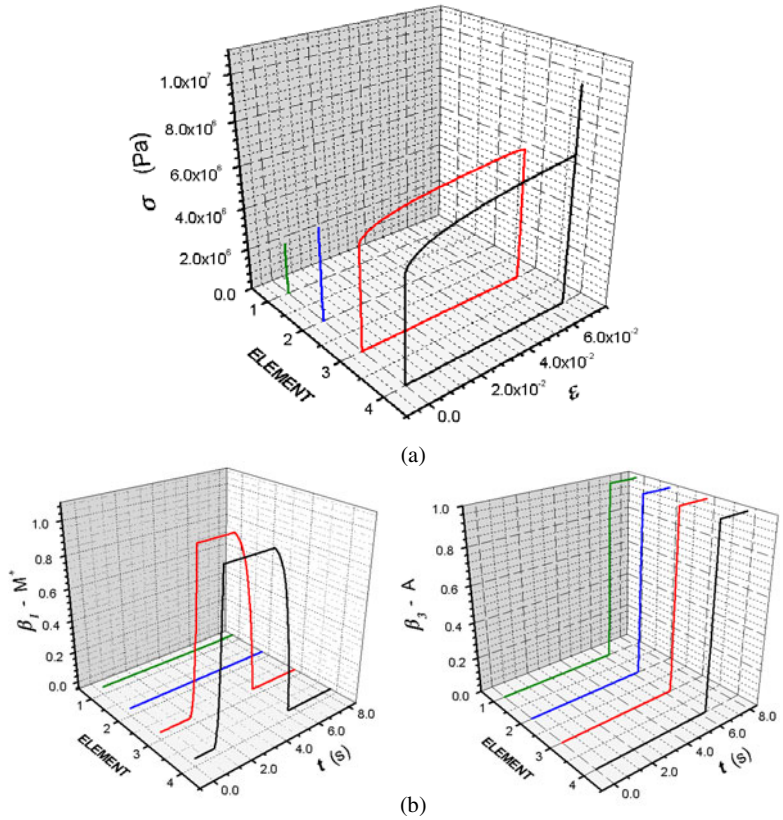

Figure 12. The shape memory effect for a bar with a variable cross-section subjected to an axial load. (a) Stress–strain curves. (b) Volumetric fractions of phases.

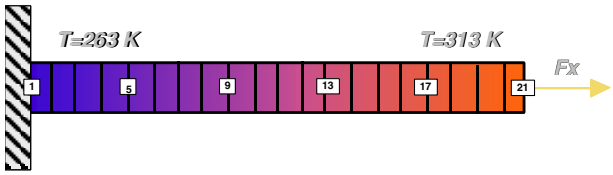

Figure 13. A bar subjected to a non-homogeneous temperature distribution.

$$(E_{\mathrm{m}}A_{\mathrm{m}} + EA_{\mathrm{a}}) \int_l (u_{,x}\,\delta u_{,x})\,\mathrm{d}x + \Lambda_{\mathrm{a}} \int_l (A_{\mathrm{a}}\delta u_{,x})\,\mathrm{d}x - \int_l (p\delta u)\,\mathrm{d}x = 0 \tag{21}$$

where A_{a} and A_{m} represent, respectively, the cross-sectional areas of the actuator and the matrix, l is the length of the bar and p is the axial load per length. Notice that the nonlinear term Λ_{a} is assumed to be constant in the actuator. The description of an entire SMA bar may be produced by considering the bar to be constructed from several actuators.

Spatial discretization is considered using the finite element method, which establishes the following approximation:

$$u(x) = \sum_{j=1}^{2} U_j^{\mathrm{e}} \vartheta_j(x) \tag{22}$$

where U_j^{e} are the element nodal displacements and $\vartheta_j(x)$ are Lagrange shape functions, presented below (Reddy 1984):

$$\vartheta_1 = 1 - \frac{x}{l} \qquad \vartheta_2 = \frac{x}{l}. \tag{23}$$

With this approximation, equation (19) is rewritten as follows:

$$(E_{\mathrm{m}}A_{\mathrm{m}} + EA_{\mathrm{a}}) \int_l [\mathbf{B_u}]^{\mathbf{T}}\,[\mathbf{B_u}]\,\mathrm{d}x\,\{\mathbf{U^e}\} + \Lambda_{\mathrm{a}} \int_l \left(A_{\mathrm{a}}\,[\mathbf{B_u}]^{\mathbf{T}}\right)\mathrm{d}x\,\{\mathbf{U^e}\} - \int_l \left(p\,[\mathbf{N_u}]^{\mathbf{T}}\right)\mathrm{d}x = 0 \tag{24}$$

which follows a discrete version of the governing equation for a generic element:

$$[K^{\mathrm{e}}]\{U^{\mathrm{e}}\} = \{F^{\mathrm{e}}\} - \{\hat{F}^{\mathrm{e}}\} \tag{25}$$

where $[K^{\mathrm{e}}]$ is the stiffness matrix, $\{U^{\mathrm{e}}\}$ is the displacement vector, $\{F^{\mathrm{e}}\}$ is the load vector and $\{\hat{F}^{\mathrm{e}}\}$ is related to the behavior of the nonlinear shape memory actuator. The definition of these matrices is as follows:

$$[K^{\mathrm{e}}] = (E_{\mathrm{m}}A_{\mathrm{m}} + EA_{\mathrm{a}}) \int_l [\mathbf{B_u}]^{\mathbf{T}}[\mathbf{B_u}]\,\mathrm{d}x \tag{26}$$

$$\{F^{\mathrm{e}}\} = \int_l \left(p[\mathbf{N_u}]^{\mathbf{T}}\right)\mathrm{d}x \tag{27}$$

$$\{\hat{F}^{\mathrm{e}}\} = \Lambda_{\mathrm{a}} \int_l \left(A_{\mathrm{a}}[\mathbf{B_u}]^{\mathbf{T}}\right)\mathrm{d}x. \tag{28}$$

After the construction of the global system, an operator split technique (Ortiz *et al* 1983) associated with an iterative numerical procedure is applied in order to deal with the nonlinearities in the formulation. First, the global vector $\hat{F}_{(i)}$, for iteration i, is evaluated assuming that neither a phase transformation nor plastic straining has taken place, which

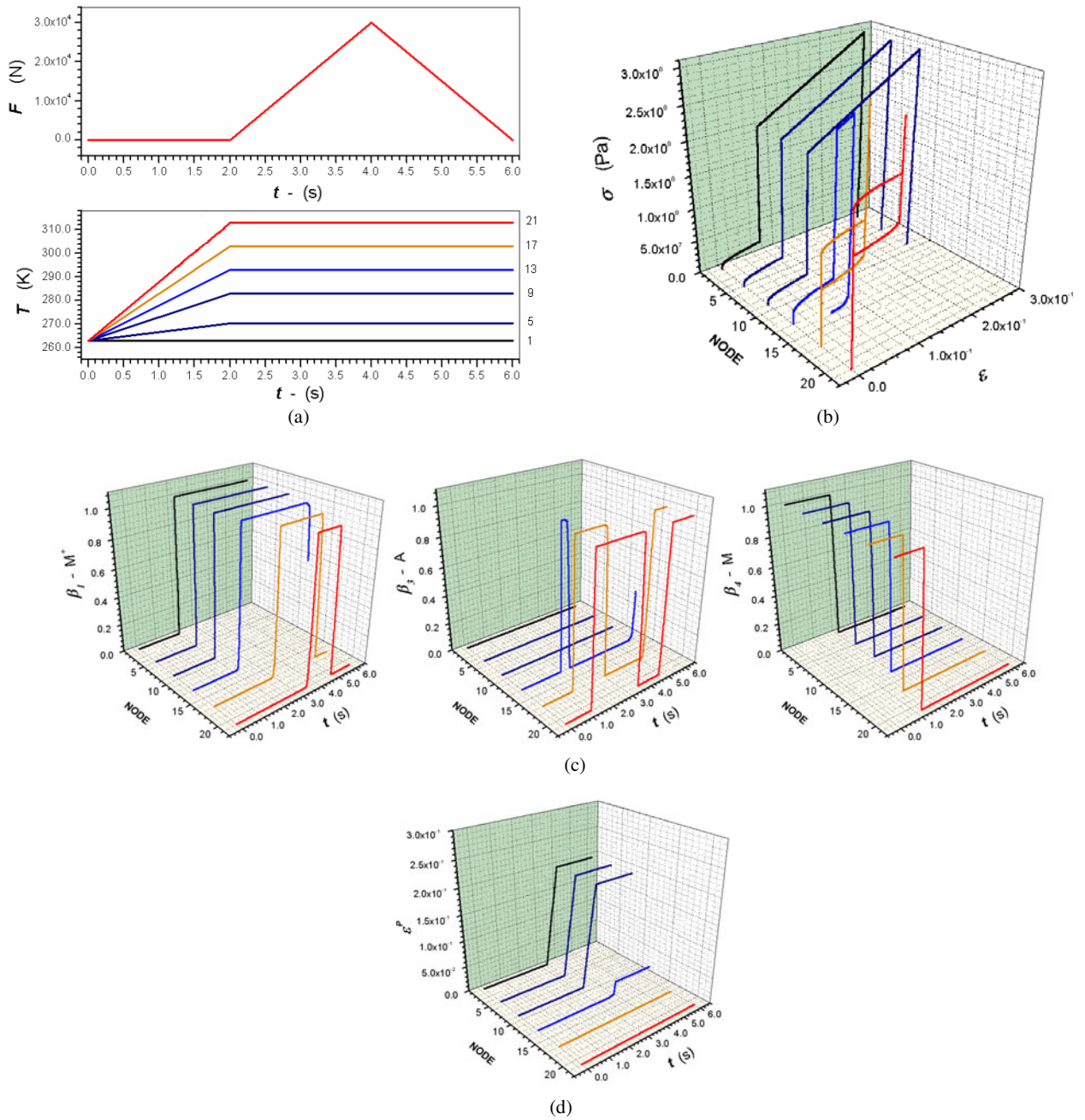

Figure 14. The response of the bar under a non-homogeneous temperature distribution. (a) Thermomechanical loading. (b) Stress–strain curves. (c) Volumetric fractions of phases. (d) Plastic strains.

means that it has the same value as in the previous time instant. Under this assumption, displacements $U_{(i)}$ are calculated by solving a linear system. In the next step, all variables related to the SMA actuator (strain, stress, volumetric fractions of the phases etc) are evaluated by considering constitutive equations.

The numerical procedure for addressing the constitutive equations uses, again, the operator split technique associated with the iterative numerical procedure. The procedure isolates the sub-differentials and uses the implicit Euler method combined with an orthogonal projection algorithm (Savi *et al* 2002). Orthogonal projections ensure that the volumetric fractions of the phases will obey the imposed constraints. In order to satisfy the constraints related to the coexistence of phases, the values for the volumetric fractions must stay inside or on the boundary of π, the tetrahedron shown in figure 1. The elastoplastic behavior is simulated with the aid of the return mapping algorithm proposed by Simo and Taylor (1986). In this algorithm, a trial state is defined by considering an elastic predictor step, using the implicit Euler algorithm to effect the time discretization of the evolution equations. If $f^{\text{trial}}_{(i+1)} \leqslant 0$, this means that the state is in the elastic domain and the trial state is the actual one. Otherwise, if $f^{\text{trial}}_{(i+1)} > 0$, we are outside the elastic domain and a plastic step must be considered. Hence, the trial state must be corrected via a projection (Simo and Taylor 1986, Simo and Hughes 1998).

After performing the evaluation of variables related to the constitutive model, the matrix $K_{(i)}$ and the vector $\hat{F}_{(i)}$ are recalculated for the next iteration. This procedure is repeated

to ensure that the norm Δ is less than a prescribed convergence tolerance:

$$\Delta = \frac{\|[\mathbf{K}']\{\mathbf{U}\} - \{\mathbf{F}\} + \{\hat{\mathbf{F}}'\}\|}{\|\{\mathbf{F}\} - \{\hat{\mathbf{F}}'\}\|} \tag{29}$$

where $\|\mathbf{v}\| = \left(\sum_{i=1}^{n} |v_i|^2\right)^{1/2}$.

It should be pointed out that the proposed model in association with classical finite element procedure allows one to analyze SMA bars. Therefore, it is possible to incorporate all potentialities of the constitutive model in the analysis of bars subjected to complex load processes.

4. Numerical simulations

This section considers numerical simulations performed using the proposed formulation. The spatial and temporal discretizations used to obtain all results given in this paper are consistent with the convergence analysis performed. The material properties are those discussed in Baêta-Neves *et al* (2004) and they are presented in table 1.

For all simulations it is assumed that $\eta_{\mathrm{ck}} = \eta_{\mathrm{ci}} = 0$. The yield limit σ_{Y} has a linear variation with T, evaluated from the following expressions:

$$T \leqslant T_{\mathrm{M}} \Rightarrow \sigma_{\mathrm{Y}} = \sigma_{\mathrm{Y}}^{\mathrm{M}} \tag{30}$$

$$T_{\mathrm{M}} < T \leqslant T_{\mathrm{A}} \Rightarrow \sigma_{\mathrm{Y}} = \frac{\sigma_{\mathrm{Y}}^{\mathrm{M}}(T_{\mathrm{A}} - T) + \sigma_{\mathrm{Y}}^{\mathrm{A,i}}(T - T_{\mathrm{M}})}{T_{\mathrm{A}} - T_{\mathrm{M}}} \tag{31}$$

$$T_{\mathrm{A}} < T \leqslant T_{\mathrm{F}} \Rightarrow \sigma_{\mathrm{Y}} = \frac{\sigma_{\mathrm{Y}}^{\mathrm{A,i}}(T_{\mathrm{F}} - T) + \sigma_{\mathrm{Y}}^{\mathrm{A,f}}(T - T_{\mathrm{A}})}{T_{\mathrm{F}} - T_{\mathrm{A}}} \tag{32}$$

where T_{A} is the temperature above which austenite is stable in the absence of stress and T_{F} is used to determine the angular coefficient of the linear interpolation.

First, a bar of SMA material with a 10 mm side square cross-section and 100 mm length is analyzed. Moreover, a homogeneous thermomechanical loading process is considered, allowing a comparison between the FEM formulation and results obtained from simulations carried out by Baêta-Neves *et al* (2004), considering a single constitutive point. The cited results were obtained using just the numerical algorithm related to the constitutive equations and, therefore, a FEM is not employed. These comparisons are used as a verification of the proposed finite element model.

Hence, consider a SMA bar with four elements (figure 3), subjected to an axial load F_x. Two different effects are treated: pseudoelastic and shape memory.

The pseudoelastic effect is now focused on, for a SMA specimen subjected to an isothermal mechanical loading performed at $T = 313$ K ($T > T_{\mathrm{A}}$). Figure 4 shows this loading process, the stress–strain curve and the evolution of the volumetric fractions of the phases. Notice that the FEM simulations and those of Baêta-Neves *et al* (2004) are in agreement. All characteristics of the constitutive model are captured by the FEM analysis. During the loading process, the specimen experiences phase transformations from the austenitic phase A to the positive martensitic variant M^+. Afterwards, during the unloading process, the reverse transformation is induced.

The shape memory effect is now focused on, in the thermomechanical loading depicted in figure 5. First, a constant temperature $T = 263$ K ($T < T_{\mathrm{M}}$) is considered, where the martensitic phase is stable. After the mechanical loading–unloading process, the specimen presents a residual strain that can be eliminated by a subsequent thermal loading (figure 5). Notice that the stress–strain curve represents the shape memory effect. Again, the FEM results and those of Baêta-Neves *et al* (2004) are in agreement except for small variations in the evolutions of the volumetric fractions of the phases. This small discrepancy is due to the different convergence criteria employed in the two models.

The phase transformation due to temperature variations is now considered for a thermal loading, depicted in figure 6, with the specimen free of stress. The response of the material under this loading process presents thermal expansion/contraction and the phase transformations. Notice the hysteretic characteristics of the phase transformation in the strain–temperature curve. Again, the FEM results and those of Baêta-Neves *et al* (2004) are in agreement.

The forthcoming analysis considers finite element simulations for different thermomechanical loads and boundary conditions. First, different boundary conditions are focused on, for a bar restricted at both ends with an axial load applied at the mid-point (figure 7). The evolution of this loading is similar to that presented in figure 4. Nevertheless, it is clear that its distribution through the bar is different. Under these conditions, different martensitic variants are induced on the left and right sides of the bar. For high temperatures, for example, the bar presents a pseudoelastic effect in all elements. However, on its left side (elements 1 and 2), a positive variant is induced (M^+), while a negative variant is induced on the right side (elements 3 and 4) (M^-). Figure 8 shows this behavior.

Similar behavior is observed for situations where a shape memory effect is of concern. With this in mind, the thermomechanical loading presented in figure 4 is considered. On the left side of the bar (elements 1 and 2) a positive variant is induced (M^+), while a negative variant is induced on the right side (elements 3 and 4) (M^-). When the mechanical loading process is finished, there are residual strains that can be eliminated by heating the bar. After this process, when the phase transformation is finished, the bar begins to present stresses due to thermal expansion since its movement is restricted by the boundary conditions. Figure 9 shows this behavior.

At this point, the behavior of a bar with variable cross-section is discussed. Figure 10 presents a representation of the beam with a square cross-section and with a height varying from 2 to 1 mm. As in the preceding example, this geometrical characteristic of the bar induces a non-homogeneous phase transformation through the length of the bar. First, consider a high temperature example. Under these conditions, phase transformations are induced in the smaller cross-sections (near the free end) where stress assumes values capable of inducing phase transformations. On the other hand, the clamped end presents an elastic response, where no phase transformation takes place (figure 11).

Similar behavior is expected for low temperatures. Under these conditions, phase transformations are induced in the smaller cross-sections (near the free end), while the bar presents an elastic response in the clamped end (figure 12).

A bar with a non-homogeneous temperature distribution is considered. Discretization is done by considering 20 elements

Table 1. Thermomechanical properties.

E_A (GPa)	E_M (GPa)	α (MPa)	α_H	L (MPa)	η (MPa K^{-1})
67	26.30	89.42	0.0637	212	0.07
T_M (K)	T_C (K)	T_0 (K)	Ω_A (MPa K^{-1})	Ω_M (MPa K^{-1})	σ_Y^M (MPa)
291.40	290.99	298	0.74	0.17	70
$\sigma_Y^{A,i}$ (MPa)	$\sigma_Y^{A,f}$ (MPa)	K_A (GPa)	K_M (GPa)	H_A (GPa)	H_M (GPa)
690	257.72	1.40	0.40	0.40	0.11

(figure 13). Figure 14 shows the thermomechanical loading process, the stress–strain curve, volumetric fractions of the phases and plastic strain time histories. The loading process begins with a thermal loading that creates a non-homogeneous temperature distribution through the length of the bar. This induces a situation where the austenitic phase (A) and twinned martensite (M) are distributed through the bar. Afterwards, a mechanical load is applied. The loading process induces the formation of a positive martensitic variant (M^+). Since the temperature distribution is non-homogeneous, different behaviors are expected through the bar. Regions with low temperatures present lower values of critical stresses, where phase transformations start. Moreover, the yield limit is also smaller and the load level causes plastification. On the other hand, for regions with higher temperatures, phase transformations start for higher stress levels and plastification does not occur. The subsequent unloading process shows that, depending on this position, there are regions with no residual strains, related to the pseudoelastic effect, and also regions that present residual strains, related to partial pseudoelastic and shape memory effects. Moreover, it should be pointed out that some regions present irreversible plastic strains.

5. Conclusions

This paper presents a nonlinear finite element analysis of shape memory bars. A constitutive model proposed by Savi *et al* (2002) and Baêta-Neves *et al* (2004) is used to describe the thermomechanical behavior of SMAs. An iterative numerical procedure based on an operator split technique is developed in order to deal with nonlinearities of the formulation. The proposed procedure allows the solution of coupled governing equations from uncoupled problems where classical procedures can be employed. Numerical simulations show that results from FEM capture the general behavior of the constitutive equation due to Baêta-Neves *et al* (2004). Moreover, other simulations show how non-homogeneous loadings can produce interesting behaviors in shape memory bars. These results indicate that the response of SMA devices subjected to non-homogeneous loadings can be very complex; this is of special interest for investigation. The authors believe that the procedure proposed in this paper could be employed as a tool to develop this investigation.

Acknowledgments

The authors acknowledge the support of the Brazilian Agencies CNPq and CAPES.

Appendix. Notation

A	Austenite phase
A_a	Actuator cross-sectional area
A_m	Matrix cross-sectional area
E	Elastic modulus
E_a	Actuator elastic modulus
E_A	Elastic modulus for the austenitic phase
E_m	Matrix elastic modulus
E_M	Elastic modulus for the martensitic phase
f	Yield surface
f^{trial}	Trail state for the yield surface
F_x	Load in direction x
H	Kinematic hardening modulus
H_A	Kinematic hardening modulus for the austenitic phase
H_M	Kinematic hardening modulus for the martensitic phase
J	Indicator function
K	Plastic modulus
K_A	Plastic modulus for the austenitic phase
K_M	Plastic modulus for the martensitic phase
L	Material parameter related to phase transformation
L_A	Material parameter related to the phase transformation associated with the austenitic phase
l	Length of the bar
L_M	Material parameter related to the phase transformation associated with the martensitic phase
M	Twinned martensite
M^+	Detwinned martensite associated with a tensile stress state
M^-	Detwinned martensite associated with a compressive stress state
p	Axial load per length
t	Time
T	Temperature
T_A	Temperature above which austenite is stable in the absence of stress
T_C	Temperature below which there is no change in the stress–strain hysteresis loop position
T_F	Temperature used to represent the yielding stress variation with temperature
T_M	Temperature below which the martensitic phase starts its formation in the absence of stress
T_0	Reference temperature
u	Displacement in the direction x
U^e	Element nodal displacement in the x direction
V	Volume
α	Material parameter that describes the martensitic transformation

α_{H}	Parameter associated with the horizontal width of the stress–strain hysteresis loop
β_i	Volumetric fraction of phase i
β_i^{S}	Value of β_i when the phase transformation of phase i begins to take place
Δ	Convergence norm
γ	Isotropic hardening variable
ε	Total axial strain
ε^{P}	Plastic axial strain
λ	Plastic multiplier
μ	Kinematic hardening variable
η	Parameter associated with the internal dissipation
η_{ci}	Parameter associated with isotropic hardening coupling
η_{ck}	Parameter associated with kinematic hardening coupling
Ω	Thermal expansion coefficient
Ω_{A}	Thermal expansion coefficient for the austenitic phase
Ω_{M}	Thermal expansion coefficient for the martensitic phase
$\vartheta_i(x)$	Lagrange shape functions
δu_i	Virtual displacement
π	Tetrahedron related to phase constraints
ρ	Density
σ	Axial stress
σ_{a}	Actuator axial stress
σ_{m}	Matrix axial stress
σ_{Y}	Yield stress
$\sigma_{\mathrm{Y}}^{\mathrm{Ai}}$	Initial yield stress for the austenitic phase
$\sigma_{\mathrm{Y}}^{\mathrm{Af}}$	Final yield stress for the austenitic phase
$\sigma_{\mathrm{Y}}^{\mathrm{M}}$	Yield stress for the martensitic phase
ψ	Helmholtz free energy
ϕ^*	Dual of the pseudopotential of dissipation
Λ_{a}	Nonlinear terms related to phase transformation and plastic behavior
$\{\mathbf{F}\}$	Global load vector
$\{\hat{\mathbf{F}}\}$	Global vector related to the behavior of the nonlinear shape memory actuator
$\{F^{\mathrm{e}}\}$	Element load vector
$\{\hat{F}^{\mathrm{e}}\}$	Element vector related to the behavior of the nonlinear shape memory actuator
$\{\mathbf{U}\}$	Global displacement vector
$\{U^{\mathrm{e}}\}$	Element displacement vector
$[\mathbf{K}]$	Global stiffness matrix
$[K^{\mathrm{e}}]$	Element stiffness matrix
$(),_x$	$\mathrm{d}(\,)/\mathrm{d}x$

References

Auricchio F and Taylor R L 1996 Shape memory alloy superelastic behavior: 3D finite element simulations *Proc. 3rd Int. Conf. on Intelligent Materials (Lyon, June 1996)*

Baêta-Neves A P, Savi M A and Pacheco P M C L 2004 On the Fremond's constitutive model for shape memory alloys *Mech. Res. Commun.* at press

Bhattacharyya A, Faulkner M G and Amalraj J J 2000 Finite element modeling of cyclic thermal response of shape memory alloy wires with variable material properties *Comput. Mater. Sci.* **17** 93–104

Birman V 1997 Review of mechanics of shape memory alloy structures *Appl. Mech. Rev.* **50** 629–45

Borden T 1991 Shape memory alloys: forming a tight fit *Mech. Engng.* **113** 66–72

Boyd J G and Lagoudas D C 1996 A thermodynamic constitutive model for the shape memory materials, part I: the monolithic shape memory alloys *Int. J. Plast.* **12** 805–42

Brinson L C 1993 One-dimensional constitutive behavior of shape memory alloys: thermomechanical derivation with non-constant material functions and redefined martensite internal variable *J. Intell. Mater. Syst. Struct.* **4** 229–42

Brinson L C and Lammering R 1993 Finite element analysis of the behavior of shape memory alloys and their applications *Int. J. Solids Struct.* **30** 3261–80

Denoyer K K, Erwin R S and Ninneman R R 2000 Advanced smart structures flight experiments for precision spacecraft *Acta Astronaut.* **47** 389–97

Duerig T, Pelton A and Stöckel D 1999 An overview of Nitinol medical applications *Mater. Sci. Eng.* A **273–275** 149–60

Fremond M 1987 Matériaux à Mémoire de Forme *C. R. Acad. Sci.* II **34** 239–44

Fremond M 1996 Shape memory alloy: a thermomechanical macroscopic theory *CISM Courses and Lectures* (Berlin: Springer)

Fujita H and Toshiyoshi H 1998 Micro actuators and their applications *Microelectron. J.* **29** 637–40

Garner L J, Wilson L N, Lagoudas D C and Rediniotis O K 2001 Development of a shape memory alloy actuated biomimetic vehicle *Smart Mater. Struct.* **9** 673–83

Kibirkstis E, Liaudinskas R, Pauliukaitis D and Vaitasius K 1997 Mechanisms with shape memory alloy *J. Physique Coll.* IV **C5** 633–6

Kouzak Z, Levy Neto F and Savi M A 1998 Finite element model for composite beams using SMA fibers *Proc. CEM NNE 98—V Congresso de Engenharia Mecânica Norte e Nordeste (ABCM) (Fortaleza, Brazil, Oct. 1998)* p 112/119

La Cava C A P L, Silva E P, Machado L G, Pacheco P M C L and Savi M A 2000 Modeling of a shape memory preload device for bolted joints *Proc. CONEM 2000—Congresso Nacional de Engenharia Mecânica (ABCM) (Natal-RN, Brazil, 2000)* (in Portuguese)

Lagoudas D C, Rediniotis O K and Khan M M 1999 Applications of shape memory alloys to bioengineering and biomedical technology *Proc. 4th Int. Workshop on Mathematical Methods in Scattering Theory and Biomedical Technology (Perdika, Greece, Oct. 1999)*

Lagoudas D C, Moorthy D, Qidwai M A and Reddy J N 1997 Modeling of the thermomechanical response of active laminates with SMA strips using the layerwise finite element method *J. Intell. Mater. Syst. Struct.* **8** 476–88

Lemaitre J and Chaboche J L 1990 *Mechanics of Solid Materials* (Cambridge: Cambridge University Press)

Liu K M, Kitipornchai S, Ng T Y and Zou G P 2002 Multi-dimensional superelastic behavior of shape memory alloys via nonlinear finite element method *Eng. Struct.* **24** 51–7

Machado L G and Savi M A 2002 Odontological applications of shape memory alloys *Rev. Bras. Odontol.* **59** 302–6 (in Portuguese)

Machado L G and Savi M A 2003 Medical applications of shape memory alloys *Braz. J. Med. Biol. Res.* **36** 683–91

Masud A, Panahandeh M and Aurrichio F 1997 A finite-strain finite element model for the pseudoelastic behavior of shape memory alloys *Comput. Methods Appl. Mech. Eng.* **148** 23–37

Ortiz M, Pinsky P M and Taylor R L 1983 Operator split methods for the numerical solution of the elastoplastic dynamic problem *Comput. Methods Appl. Mech. Eng.* **39** 137–57

Pacheco P M C L and Savi M A 1997 A non-explosive release device for aerospace applications using shape memory alloys *Proc. COBEM-97, XIV Congresso Brasileiro de Engenharia Mecânica (ABCM) (Bauru, São Paulo, Nov. 1997)*

Pietrzakowski M 2000 Natural frequency modification of thermally activated composite plates *Mec. Ind.* **1** 313–20

Reddy J N 1984 *An Introduction to the Finite Element Method* (New York: McGraw-Hill)

Rogers C A 1995 Intelligent materials *Sci. Am.* (September) 122–7

Savi M A, Braga A M B, Alves J A P and Almeida C A 1998 Finite element model for trusses with shape memory alloy actuators *EUROMECH 373 Colloquium—Modeling and Control of Adaptive Mechanical Structures (Magdeburg, March 1998)*

Savi M A, Paiva A, Baêta-Neves A P and Pacheco P M C L 2002 Phenomenological modeling and numerical simulation of shape memory alloys: a thermo-plastic-phase transformation coupled model *J. Intell. Mater. Syst. Struct.* **3** 261–73

Simo J C and Hughes T J R 1998 *Computational Inelasticity* (Berlin: Springer)

Simo J C and Taylor R L 1986 A return mapping algorithm for plane stress elastoplasticity *Int. J. Numer. Method. Engng.* **22** 649–70

Tanaka K 1986 A thermomechanical sketch of shape memory effect: one-dimensional tensile behavior *Res. Mech.* **18** 251–63

Trochu F and Qian Y-Y 1997 Nonlinear finite element simulation of superelastic shape memory alloy parts *Comput. Struct.* **62** 799–810

Trochu F, SacéPé N, Volkov O and Turenne S 1999 Characterization of NiTi shape memory alloys using dual kriging interpolation *Mater. Sci. Eng.* A **273–275** 395–9

Trochu F and Terriault P 1998 Nonlinear modelling of hysteretic material laws by dual kriging and application *Comput. Methods Appl. Mech. Eng.* **151** 545–58

van Humbeeck J 1999 Non-medical applications of shape memory alloys *Mater. Sci. Eng.* A **273–275** 134–48

Webb G, Wilson L, Lagoudas D C and Rediniotis O 2000 Adaptive control of shape memory alloy actuators for under water biomimetic applications *AIAA J.* **38** 325–34